Ingeniería 27 (1): 21-38, ISSN: 2215-2652; 2017. San José, Costa Rica

Effect of preparation method on catalytic activity of Ni/ γ-Al_2O_3 catalysts

Efecto del método de preparación sobre la actividad catalítica de catalizadores de Ni/ γ-Al_2O_3

Ing. Bárbara Miranda Morales, Ph. D.
Universidad de Costa Rica, San José, 2060, Costa Rica
barbara.mirandamorales@ucr.ac.cr

Recibido: *9 de febrero 2016* ***Aceptado:*** *8 de agosto 2016*

Abstract

The performance of catalysts has been shown to be strongly dependent on their methods of preparation. A study to examine the relationship between catalyst preparation procedures and the structure, dispersion, activity, and selectivity of the finished catalyst is reported. 10 wt.% Ni/γ-Al_2O_3 catalysts were prepared by incipient wetness impregnation and by wet impregnation. The catalysts were used in the conversion of glycerol in gas phase and atmospheric pressure. The selectivity and activity of the catalysts were affected by the preparation method employed. The catalysts were characterized by TGA, TPR, N_2-physorption, H_2-chemisorption, XRD, TEM, FTIR and TPO. The Ni particle size and dispersion of the catalysts affected the selectivity to hydrogenolysis and dehydration routes, and the formation of carbon deposits was also affected.

Keywords:
Atmospheric pressure, nickel, glycerine, adsortion, hydrogenolysis, catalyst.

Resumen

Se ha demostrado que el desempeño de los catalizadores está fuertemente ligado a los métodos de preparación. En este artículo se reporta un estudio de la relación entre el método de preparación y la estructura, la dispersión, la actividad, y la selectividad de catalizadores de Ni/γ-Al_2O_3. Los catalizadores fueron preparados por impregnación seca y por impregnación húmeda. Las muestras fueron usadas en la reacción de conversión de glicerol en fase gas y a presión atmosférica. Los catalizadores fueron caracterizados mediante TGA, TPR, N_2-fisisorción, H_2-quimisorción, XRD, TEM, FTIR y TPO. El tamaño de la partícula de Ni y la dispersión afectaron la selectividad de los catalizadores hacia las rutas de hidrogenólisis y deshidratación, la formación de depósitos de carbón sobre los catalizadores se vio afectada también.

Palabras clave
Presión atmosférica, níquel, glicerina, adsorción, hidrogenolisis, catalizadores.

1. INTRODUCTION

Supported nickel catalysts have been used in processes such as the CO methanation (1) and the hydrogenolysis of glycerol to added-value products (2). The behaviour of catalysts is dependent on the preparation conditions as well as pretreatment procedures (3). A general preparation procedure to form these supported nickel catalysts includes the steps of impregnation, drying, dehydration, activation (calcination/reduction), and passivation. Each step in this preparation sequence has been shown to affect the performance of the finished catalyst (4, 5). For example, Bartholomew and Farrauto (1976) (6) have demonstrated that the calcination temperature, heating rate during reduction, reduction temperature, hydrogen space velocity used in reduction, nickel weight loading, and passivation procedures all affect the nickel surface area and percentage reduction of nickel oxide to nickel metal when the Ni/γ-Al_2O_3 catalysts are prepared from nickel nitrate by wet impregnation techniques. They indicated that controlled decomposition of alumina-supported nickel nitrate in a hydrogen atmosphere tends to maximize nickel surface area, dispersion, and reduction to nickel metal (6). Wang *et al*. (1998) (7) investigated the effects of the support phase and catalyst preparation methods on catalytic activity and carbon deposition over nickel catalysts supported on Al_2O_3, SiO_2 and MgO for the reforming reaction of methane with carbon dioxide. It is found that the pore structure of the support and metal-support interaction significantly affected the catalytic activity and coking resistance. Strong interaction between metal and the support made the catalyst more resistant to sintering and coking, thus resulting in a longer time of catalyst stability.

Catalytic studies have shown that significant differences result when the weight loading of nickel on the alumina carrier is varied. Huang *et al*. (1986) (3) studied the effect of solutions variables on metal weight loading during catalyst preparation. Ni/γ-Al_2O_3 catalysts were prepared by wet impregnation with three different metal loadings (5,8 %, 2,9 %, and 0,7 % wt.). The combined effects of pH and ionic strength of the impregnation solution where demonstrated to change the amount of catalytic precursors sorbet on the support.

The particle size in supported metal catalysts is an important parameter controlling the surface structure of the metal particles and these changes in the surface structure are reflected in both the specific activity and the chemisorption properties (8). Frelink *et al*.(1995) (9) studied the effect of the particle size of carbon-supported Pt catalysts on the electrooxidation of methanol. Different methods were used to prepare Pt/C catalysts with particle sizes ranging between 1,2 nm and 10 nm. The specific activity was found to decrease with decreasing particle size in the range 4,5 nm-1,2 nm. The dependence of the activity on the particle size can be explained in terms of either its effect on the formation of an adsorbed hydroxy species or its effect on the number of methanol adsorption sites. Moreover, the surface area, pore structure and nature of the support on one hand, and the preparation method on the other, strongly affect the ultimate particle size with dispersed metal catalysts. These factors can be controlled via the preparation and the pretreatment of the catalysts. With nickel catalysts it has been demonstrated that the method of preparation strongly influences the reducibility of the nickel ions. Catalysts prepared

by precipitation and, particularly, those by coprecipitation, are more difficult to reduce than impregnated ones are (10), exhibiting an extensive metal-support interaction, generally of an electronic type. Thus, the supported nickel catalysts are usually prepared by impregnation of the support with a solution of the metal salt until incipient wetness. In this way, the precursor of the active component is uniformly distributed in the pore volume of the carrier (3, 11-16).

Activity, is a structure-sensitive catalytic property (17). Structure is normally defined as the atomic arrangement at the surface. For a supported metal catalyst, the structure of the surface is, therefore, determined by the arrangement among metal, support and metal-support compound(s). Interactions between the metal and the support are expected to affect these arrangements and the resulting surface structure (17, 18). Different types and sizes of reaction centers and their associated chemical environments are expected for systems with varying extents of metal-support interaction. In a heterogeneous catalytic reaction, the reaction is normally carried out on the catalytic centers, and the reaction rate is likely to be very sensitive to any variation in structure of the reaction centers and their chemical environment. The difficulty in the reduction of the supported catalysts is reportedly due to the interaction of the small highly dispersed crystallites with the alumina support. This hypothesis is further supported by the fact that the nickel particle sizes as determined by hydrogen TPD are larger for catalysts prepared by incipient wetness compared to those catalysts prepared by wet impregnation at comparable metal loading (19). The more uniform and larger "particle-like" nickel geometry are, therefore, more fully developed on the catalysts prepared by incipient wetness than those catalysts prepared by wet impregnation (19, 20).

Y.-J. Huang *et al*. (1987) (21) demonstrate that the methanation activity for the Ni/Al_2O_3 catalysts prepared by wet impregnation have higher activity than those prepared by incipient wetness. The results show that the catalysts prepared by wet impregnation have higher dispersion than those prepared by incipient wetness. The catalytic properties of the catalysts with different crystallite size would be different (22). In light of the results, the larger the difference in crystallite size, the larger the difference in activity (21).

A. Gurbani *et al*. (2009) (23) studied the effects of the preparation methods on the performance of Cu-Ce catalyst for the selective oxidation of CO, and its relationship with textural and structural properties. Two catalysts were prepared using impregnation and deposition–precipitation methods. The metallic copper crystallite size for Cu–Ce WI and Cu–Ce DP, which was estimated by CO chemisorption, was 3,2 nm and 1,2 nm, respectively. The activity results confirm the worse performance of Cu–Ce prepared by DP especially when oxygen is not in excess (23).

The overall objective of this research is to examine the relationship between catalyst preparation procedures and the structure, dispersion, activity, and selectivity of the finished catalyst.

2. METHODOLOGY

2.1 Catalyst preparation

Commercial γ-Al_2O_3 was purchased from Degussa and was calcined at 463 K for 4 h before use. The samples containing 10 wt.% of Ni were prepared by incipient wetness impregnation and wet impregnation of γ-Al_2O_3 with a $Ni(NO_3)_2.6H_2O$ (Aldrich, 99.999%) aqueous solution. After impregnation the samples were dried at 373 K for 12 h and then reduced at 723 K in a flow of 20 mL/min with pure H_2 for 4 h. The resultant material was labeled as Ni_{inc} and Ni_{wet}, respectively.

2.2 Catalyst Characterization

The decomposition temperature of $Ni(NO_3)_2.6H_2O$ precursor was investigated by TGA over dried sample after impregnation of the Ni precursor aqueous solution. TGA were recorded in a Labsys/Setaran TG thermo balance apparatus from room temperature (RT) to 1173 K, at a heating rate of 10 K/min under a flow of 5 % H_2/Ar. TPR experiments were performed in a ThermoFinnigan (TPORD 110) apparatus equipped with a thermal conductivity detector (TCD). The samples were then purged with argon flow before the TPR. The analysis was carried out using a 5 % H_2/Ar gas flowing at 20 ml/min by heating from RT to 1173 K with a heating rate of 10 K/min. The specific surface areas, cumulative pore volumes and average pore diameters of the samples were measured by the BET method using N_2 adsorption/desorption at 77 K in a Quantachrome Autosorb-1. Before measurement, each sample was degassed under vacuum at 393 K for10 h. TEM study was carried out in a JEOL JEM-2100 instrument operating at an accelerating voltage of 100 kV. The samples were prepared by dispersing the as-prepared catalysts in alcohol and then dropping the aqueous suspension on a standard 3 mm holey carbon-coated copper grid and letting the water evaporate at RT. H_2-chemisorption was performed to determine the total area of the exposed metallic Ni atoms (24). The analysis was performed using a conventional static method in a Micromeritics 2010 instrument. The samples were heated in flowing He at 400 K for 1 h; then the temperature was increased to 723 K. At this temperature, the He flow was replaced by H_2 flow, and the samples were reduced for 2 h and subsequently out-gassed for 30 min. Finally, the samples were cooled to RT and evacuated at RT for 30 min. The hydrogen adsorption isotherm was recorded at RT. After evacuation at RT for 10 min, a second H_2 isotherm was obtained. The chemisorbed H_2 uptake was obtained by extrapolating to zero pressure the linear portion of the isotherm. The number of exposed Ni atoms was calculated assuming spherical particles, the stoichiometry factor of 1 atomic chemisorbed hydrogen per surface Ni atom, a Ni surface area of 0,065 nm^2 per Ni atom and a Ni density of 8,9 g/cm^3 (24). The total acidity measurements of the fresh catalysts were determined by TPD of NH_3 on a ThermoFinnigan TPDRO 1100 equipped with a TCD detector. Each sample (0,1 g) was pretreated with Ar at 353 K during 1 h in a tubular down-flow quartz reactor and then cooled to RT. The sample was then treated with NH_3

flow (5 % NH_3 in He) at RT for 1 h. The NH_3 desorption was measured by heating the sample from RT to 1073 K at a rate of 5 K/min in He flow. The total number of acid sites was calculated by using pulses of a known amount of NH_3. The XRD analysis of the materials was recorded using a Siemens D5000 diffractometer (Bragg-Bentano for focusing geometry and vertical θ-θ goniometer) with an angular 2θ-diffraction range between 5º and 70º. The samples were dispersed on a Si (510) sample holder. Spectra were collected with an angular step of 0,03º at 5 s per step of sample rotation. Cu Kα radiation (λ=1,54056 Å) was obtained from a copper X-ray tube operated at 40 kV and 30 mA. FTIR of adsorbed CO was carried out with a Nicolet Magna 750 spectrometer equipped with an MCT detector operating at 4 cm^1. The in situ infrared cell used in the experiments was a 2¾ in six-way stainless steel cube equipped with KBr IR-windows. The cell is connected to a gas handling/pumping station and through both leak and gate valves to a quadrupole mass spectrometer (UTI 100C). The sample was pressed onto a fine tungsten mesh, which, in turn was mounted onto a copper sample holder assembly attached to ceramic feedthroughs of 0,034 m flange. The sample temperature was monitored through a chromel/alumel (K-type) thermocouple spot-welded to the top center of the tungsten mesh. Prior to the measurements, the sample was heated to 723 K and kept in this temperature for 2 h to ensure the removal of all water from the catalyst. Then, the sample was reduced with H_2 at 723 K using two cycles. First cycle was for 30 minutes and the second cycle for 10 minutes. The cell was evacuated after each reduction cycle. The base pressure of the cell was less than $1,33x10^{-4}$ Pa. Finally, the sample was cooled down to 300 K for the CO adsorption measurements. Prior to each spectral series acquisition, a background spectrum was taken of the fresh sample. For each sample, the adsorption of CO was performed by increasing the final equilibration CO pressure in the cell to around 47 Pa. Finally, the FTIR spectra of adsorbed CO were recorded. The amounts of coke deposited on the spent catalysts were determined by TPO. These tests were carried out with a Sensys Evo apparatus. TPO profiles were obtained from approximately 20 mg of sample, placed in a quartz reactor (ID= 0,5 cm, length = 10 cm) and heated from 303 K to 1023 K at a rate of 10 K/min in air flow. The CO_2 produced was quantified on-line using a Pfeiffer Vacuum QME 220 mass spectrometer.

2.3 Conversion of glycerol

The catalytic conversion of glycerol was carried out in gas phase in a quartz fixed bed down flow reactor at 573 K for 6 h. Gas flow rates were controlled by unit mass flow controllers. The feed gas composition during reaction was 5 % H_2 in Ar. An aqueous solution of glycerol (3 v/v %) was pumped by a syringe pump with flow of 3,5 mL/h and injected into the reactive gas. Previous to entrance to the reactor the reactive mixture was preheated at 573 K. Hydrogen/Glycerol molar ratio of 10 was used in all experiments. Typically 100 mg of sample in the form of pellets, with size ranging 2 mm– 3 mm, were loaded in the quartz reactor and the reactor was heated to the desired temperature. The condensed products were trapped in an ice bath condenser and analyzed by HPLC every 20 minutes of reaction in a high performance liquid Chromatography (HPLC, Agilent technologies 1100 series) equipped with a ICSep ICE-COREGEL 87H3 Column serial

Nº 12525124 column, a diode-array detector (DAD) and a refractive index (RID) detector. The mobile phase was deionized and filtered water with pH controlled to 2,2 by addition of sulfuric acid with flow of 0,6 ml/min and a pressure of 50 bar. The temperature of the HPLC column was 313 K and 50 minutes of analysis for each chromatogram. The gaseous products were continuously analyzed by an on-line gas chromatograph equipped with a FID detector and a HP Poraplot column (30 m×0,53 mm×0,6 m). Finally, a total organic carbon (TOC) analyzer was used to check the carbon balance. The TOC analysis was performed on a Shimadzu TOC-5000A using high purity air (pressure of 400-500 kPa and flow rate of 150 mL/min) and a furnace temperature of 953 K. The conversion of the glycerol was defined as follows:

$$Conversion\ of\ \text{glycerol}\,(\%) = \frac{Moles\ of\ glycerol\ reacted}{Initial\ moles\ of\ glycerol}\ x\ 100$$

The selectivity to each product was defined as selectivity based on carbon, where:

$$Selectivity\ (\%) = \frac{Moles\ of\ carbon\ in\ specific\ product}{Moles\ of\ carbon\ in\ all\ \ products}\ x\ 100$$

3. RESULTS AND DISCUSSION

3.1. Catalyst Characterization

3.1.1 Thermal decomposition of $Ni(NO_3)_2.6H_2O$ impregnated over γ-Al_2O_3

In Fig. 1. is shown the thermogravimetric analysis curves of Ni_{inc} and Ni_{wet}, the main decomposition of $Ni(NO_3)_2.6H_2O$ under H_2/Ar occurred below 620 K for both samples.

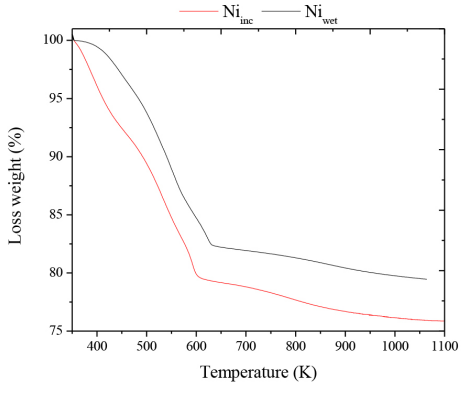

Figure 1. Thermogravimetric analyses for the Ni samples.

The TPR profiles of the Ni samples in Fig. 2 show two peaks. The first evolutions of hydrogen consumption were observed between 500 K and 620 K which corresponds to the decomposition of nickel nitrate precursor to the nickel oxide species, in accordance with previous work (25-28). The broad peak between 600 K and 1000 K indicate the reduction of the NiO species with different interaction with the support (28-31). It can be seen that the TPR profile of the Ni_{wet} sample show peaks at lower temperatures (574 K and 749 K) than the Ni_{inc} sample (600 K and 750 K, 800 K) which could be due to the difference in particle size as was determined by TEM.

The $Ni(NO_3)_2.6H_2O$ impregnated over γ-Al_2O_3 sample was characterized by in situ XRD and XANES as was discussed in previous articles (2, 32). In situ XRD showed that the total decomposition of the Jamborite phase occurred around 600 K in agreement with TGA of Fig. 1. The Ni K-edge temperature resolved XANES spectrum and the distribution of Ni species with temperature for the in situ reduction of $Ni(NO_3)_2.6H_2O$-impregnated over γ-Al_2O_3 showed that between 650 K and 920 K occurred all the formation of metallic Ni (2). In this study, the Ni catalysts were reduced at 723 K because of the information obtained from a previous work where the Ni723 catalysts had the highest number of exposed Ni atoms and the increase in the reduction temperature to 823 K-1073 K provoked a decrease in the dispersion and sintering of the Ni particles (2).

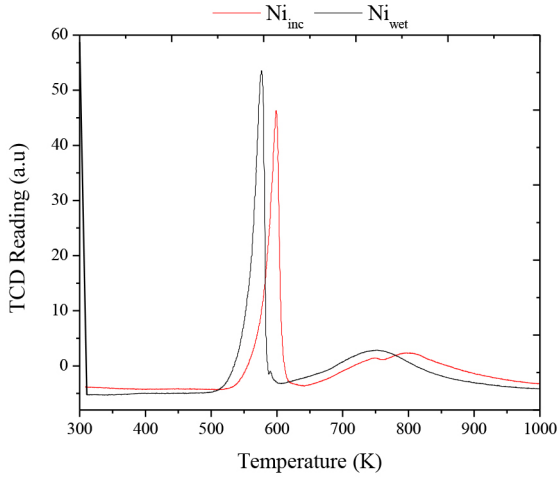

Figure 2. H_2-TPR analyses for the Ni samples.

3.1.2 X-ray diffraction

XRD patterns of the fresh Ni samples (Fig. 3) were recorded in order to identify the crystalline phases formed after the reduction at 723 K under H_2 flow of the impregnated samples. Two distinct crystallographic phases are observed, which correspond to metallic Ni, and the corresponding γ-Al_2O_3 phase (ICDD 79-1558) of the support. It can be seen that the metallic Ni diffraction peaks are broad and of low intensity, indicating that the Ni metal particles are highly dispersed on the γ-Al_2O_3 support in the fresh catalysts. The

peaks at around 2θ= 37,5°, 45,7° and 66,7° are assigned to the γ-Al_2O_3 phase. The other broad peak at around 2θ = 44,5° is attributed to Ni (111) (28, 33). For the Ni_{wet} sample diffraction peaks of Ni species are not observed. The lack of Ni-related reflections in this sample can be attributed to highly dispersed Ni atoms. The NiO phase (Bunsenite, ICDD 47-1049) was not detectable in any samples. In this study, the Ni catalysts were reduced at 723 K and from previous XANES results, the Ni content was not completely reduced to metallic Ni at this temperature (723 K), consequently, the presence of nickel oxides phases not detected by XRD should not be discarded (2).

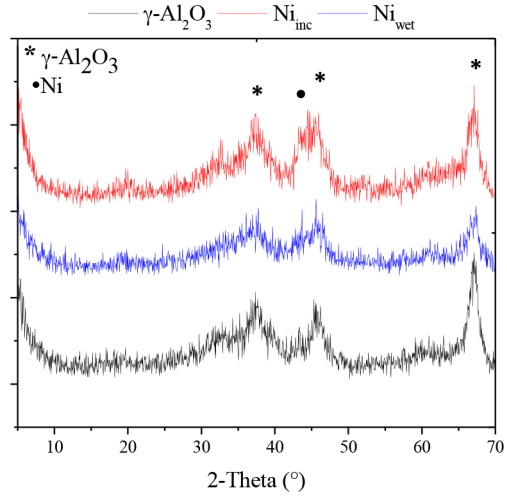

Figure 3. X-ray diffraction patterns of the fresh Ni samples and the γ-Al_2O_3 support.

3.1.3 TEM

The morphology and the metal particle size of the fresh Ni/γ-Al_2O_3 catalysts were characterized by TEM (Fig. 4). The Ni_{inc} catalyst contains small Ni particles with sizes ranging between 4 nm-10 nm with a mean particle size of 6 nm (Figs. 4a and 4b). For Ni_{wet} catalyst TEM images show Ni particles well distributed over the γ-Al_2O_3 support (Figs. 4c and 4d) with Ni particle size ranging between 4 nm–6 nm in diameter indicating that the wet impregnation method produce smaller particle size than the incipient wetness impregnation method.

3.1.4 N_2-physisorption

The N_2-physisortion results of the Ni samples are depicted in Table 1. The γ-Al_2O_3 support presents a surface area of 113 m^2/g and pore volume of 0,20 cm^3/g. The BET surface area of the Ni_{wet} sample decreased a little bit (108 m^2/g) in comparison with the support and the Ni_{inc} BET area decreased until 99 m^2/g. The pore volume was of

0,17 cm^3/g for both Ni catalysts. The higher BET surface area of the Ni_{wet} sample is in accordance with its lower particle size from TEM results.

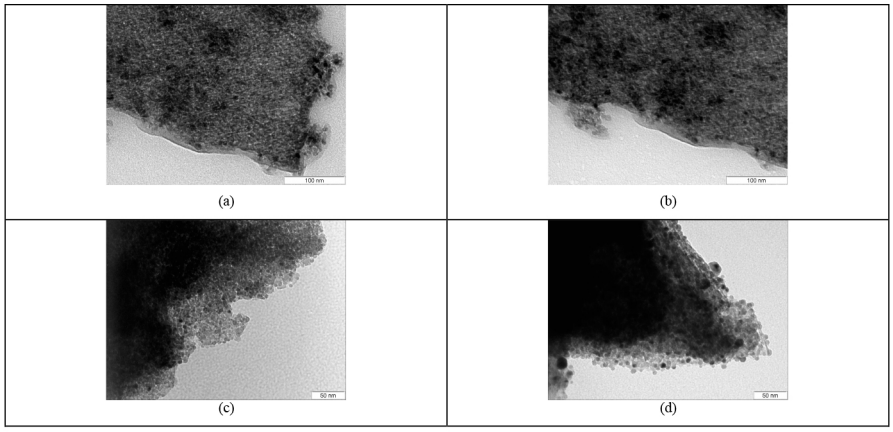

Figure 4. TEM images of the fresh (a, b) Ni_{inc}, and (c, d) Ni_{wet} samples.

Table 1 Textural and physical-chemical properties of fresh Ni catalysts and γ-Al_2O_3 support.

Sample	**SBET (m^2/g)**	**Pore volume (cm^3/g)**	**Pore size (nm)**	**NH_3-TPD ($\mu mol/g_{sample}$)**	**Number of exposed Ni atoms**
γ-Al_2O_3	113	0,20	4,54	182,1	-
Ni_{inc}	99	0,17	4,54	205,4	3,43 x 1019 (33%)[a]
Ni_{wet}	108	0,17	4,15	224,5	9,22 x 1019 (82 %)[a]

a: Percentage of exposed Ni atoms

The N_2 adsorption-desorption isotherms of the Ni supported on γ-Al_2O_3 are shown in Fig. 5a. Both Ni catalysts exhibit the type IV isotherm according to the Brunauer-Deming-Deming-Teller (BDDT) classification, which exhibits the condensation and evaporation step characteristic of mesoporous materials. All isotherms at low equilibrium pressures are reversible, whereas at higher equilibrium pressures they exhibit a hysteresis loop of the H_3 type (34). The pore diameter distribution curves of the Ni samples are shown in Fig. 5b. The Ni samples present a pore diameter in the range between 4,0 nm and 4,5 nm.

3.1.5 NH_3-TPD

The Ni incorporation to the support produces a little increase in the strong Lewis acid sites (205,4 $\mu mol/g_{sample}$ and 224,5 $\mu mol/g_{sample}$) compared with the correspondent bare alumina (182,1 $\mu mol/g_{sample}$). The amounts of desorbed NH_3 measured by volumetric adsorption are depicted in Table 1 for all the samples. The surface acidity was calculated as total acidity and expressed per mol of NH_3 desorbed per gram of sample. The

total acidity results show that in this case, the acidity of the catalysts was not affected by the preparation method.

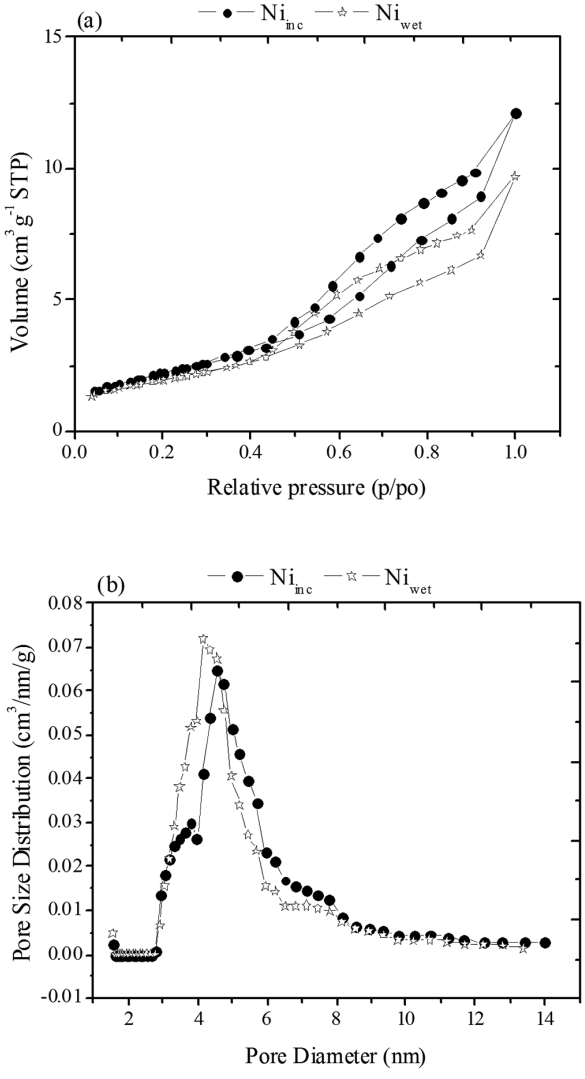

Figure 5. (a) N_2-physisorption isotherms, and (b) Pore size distribution of the fresh Ni/γ-Al_2O_3 samples

3.1.6 H_2-Chemisorption

Table 1 shows the number of exposed Ni atoms and the percentage of exposed Ni atoms, as determined by H_2-chemisorption. The Ni_{inc} sample has fewer exposed Ni atoms than the Ni_{wet} sample (33 % and 82 %, respectively). We must remind that the Ni_{wet} sample presented a higher BET surface area and a lower particle size than the Ni_{inc} sample which is in agreement with its higher dispersion.

3.2 Conversion of glycerol

The catalytic performance of Ni/γ-Al_2O_3 catalysts prepared by different procedures was evaluated in the conversion of glycerol under atmospheric pressure and 573 K. The catalytic performance for Ni catalysts is shown in Fig. 6. It shows a decrease in glycerol conversion with time on stream for Ni_{inc} sample, the deactivation was pronounced for this sample. For the Ni_{wet} sample the glycerol conversion was about 100 % over 6 h of reaction indicating high stability of the catalyst.

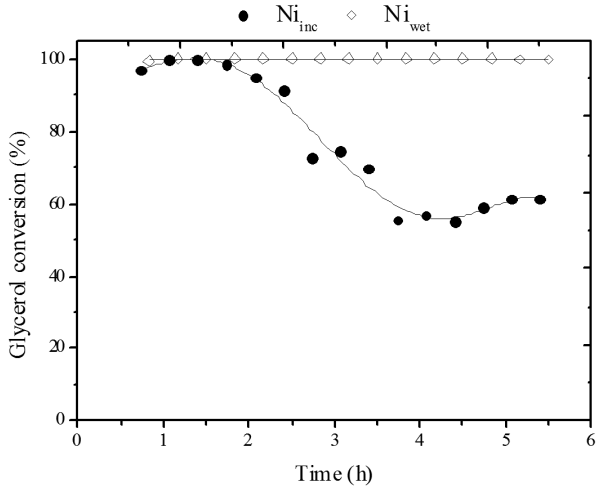

Figure 6. Catalytic performances of the Ni catalysts in functionof time of reaction.

The effect of bifunctional metal-acid properties of the Ni catalysts can be seen in two main routes (i) the hydrogenolysis of glycerol to methane and acetaldehyde and (ii) dehydration-dehydrogenation to the production of hydroxyacetone, pyruvaldehyde, pyruvic acid, methyl lactate and lactide (2). The selectivity profiles of the different products obtained for the Ni samples are shown in Fig. 7. The main products in the condensable phase observed during conversion of glycerol were: hydroxyacetone, pyruvaldehyde, pyruvic acid, lactic acid, lactide, ethylene glycol (EG), acetaldehyde, and methyl lactate. The major products detected in the gas phase were methane (CH_4), acetaldehyde, and traces of formaldehyde, propanal and acetone.

The catalyst deactivation shown in Fig. 6 affected the selectivity during the glycerol conversion for the Ni_{inc} sample (Fig. 7a). The selectivity to hydrogenolysis products such as CH_4 decreases meanwhile the products of dehydration and dehydrogenation increase. For instance, for the Ni_{inc} sample, the selectivity to hydroxyacetone and lactide increased from 10,6 % to 15,4 % and 14,6 % to 27,7 %, respectively, with raising reaction time from 2 h to 4 h, while the selectivity to CH_4 decreased from 100 % to 20 % at 4 h of reaction. It is important to note that esterification products such as methyl lactate and methyl pyruvate are observed when both routes of hydrogenolysis and dehydration-dehydrogenation are present (2). In the case of the Ni_{wet} catalyst (Fig. 7b) the selectivity to CH_4 was practically 100 % during the 6 h of reaction. A previous work (2) revealed that

in the case of glycerol hydrogenolysis, the number of exposed Ni atoms determined the production of CH_4 and acetaldehyde, the higher the total number of exposed Ni atoms higher is the CH_4 selectivity. Ni_{wet} sample exhibit a higher hydrogenolytic capacity due to its highest number of exposed Ni atoms of $9{,}22x10^{19}$ in comparison with $3{,}43x10^{19}$ of the Ni_{inc} sample. The metal property was remarkable for the Ni_{wet} sample inducing the presence of the hydrogenolysis route. Indeed the Ni_{wet} sample not showed selectivity to products such as pyruvaldehyde, lactide and hydroxyacetone due to its higher hydrogenolytic capacity.

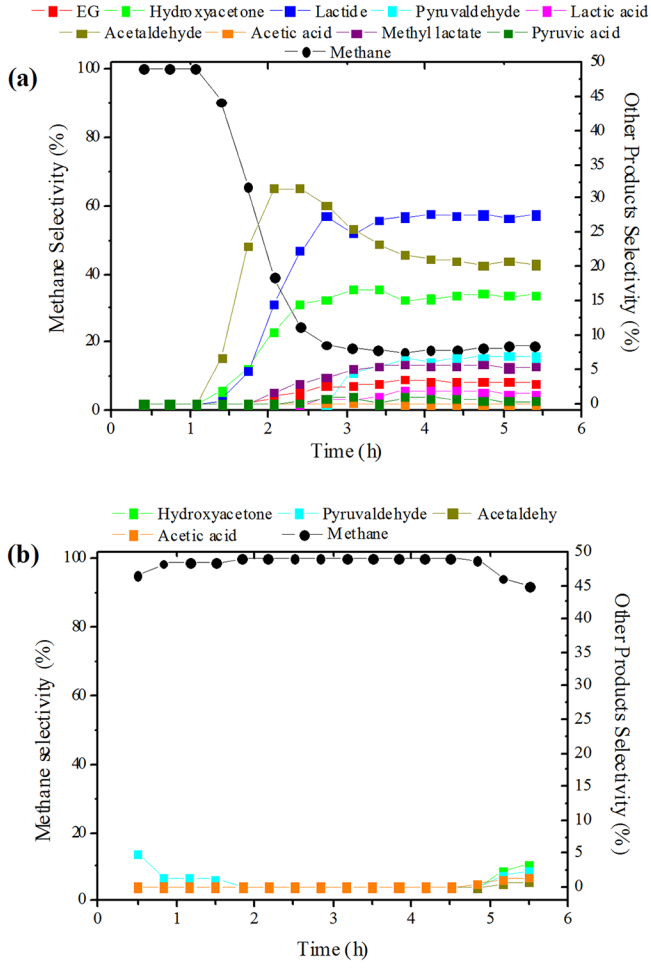

Figure 7. Time-on stream product selectivity in glycerol conversion over (a) Ni_{inc} and (b) Ni_{wet}

Fig. 8 shows the IR spectra of adsorbed CO on Ni samples at RT after reduction at 723 K. The spectra displayed were obtained after different CO doses and evacuation in order to eliminate the gas phase species. The CO adsorption band at 2130 cm^{-1} is attributed to CO polarized by Ni^{2+} ions. The observed band at 2072 cm^{-1} is ascribed to subcarbonyl species, and the band at 2049 cm^{-1} can be related to linear Ni^0-CO species (35) in agreement with Blackmond and Ko (36). The bands at 1955 cm^{-1} and 1910 cm^{-1}

can be assigned to CO molecules bridged bounded to Ni atoms. The band at 1791 cm^{-1} is attributed to Ni_3CO and Ni_4CO species (nickel carbonyl species) (37).

In a previous work (32) was observed that the addition of Cu to Ni catalysts resulted in the elimination of CO molecules bridged–bonded to metallic Ni as the Ni/Cu atomic ratio decreased. The effect of Cu on Ni/γ-Al_2O_3 observed was attributed to geometrical effect and/or change in electronic properties. The geometric effect would affect the number of Ni sites available for adsorption. The H_2-chemisorption results suggested that Cu was the predominant component in the surface of the catalyst as the Ni/Cu atomic ratio decreases. XPS results showed that Cu progressively covered the Ni atoms. In these regards the activity of Ni atoms towards CH_4 formation was greatly affected and this effect was explained by a geometrical effect of dilution of the active hydrogenolysis Ni sites by the presence of Cu atoms (38-40). The geometrical effect was clearly noted by the FTIR of adsorbed CO results revealing the progressive elimination of CO molecules bridge bounded to Ni atoms which are observed at the low frequency band 2000 cm^{-1}–1800 cm^{-1}. In this respect, the active Ni sites for rupture of C-C bond of glycerol may require a large ensemble of atoms. Adjacent Ni atoms on the catalyst surface can form suitable ensemble for the hydrogenolysis route (32). In this way, the stability of the Ni_{wet} sample in the CH_4 production during glycerol reaction could be an effect of the presence of a suitable array of active Ni atoms to accommodate the reactive molecule as was observed in the highest dispersion of the Ni_{wet} sample by H_2-chemisorption results. The Ni_{inc} sample has a lower ($3{,}43x10^{19}$) number of exposed Ni atoms.

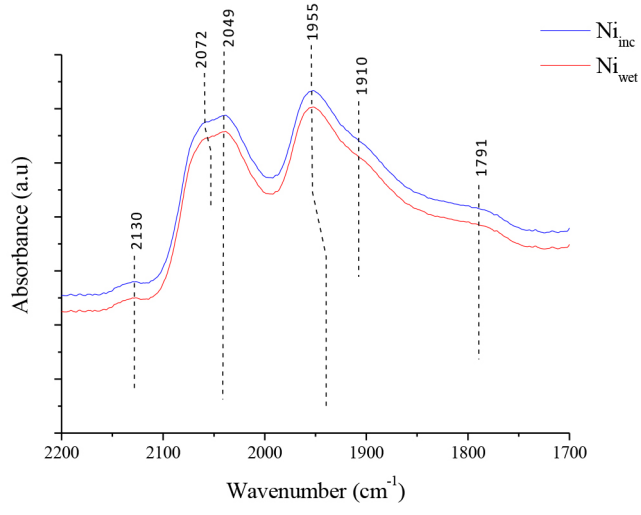

Figure 8. Infrared spectra of reduced Ni catalysts after evacuation of CO.

On the other hand, the acid property of the Ni catalysts plays a role of dehydration on the catalytic performance as was shown in a previous work (2) where the highest acidity (273,1 mol/g_{sample}) of the Ni623 sample favored the formation of hydroxyacetone and suppressed the formation of CH_4. As can be observed in Table 1, the Ni_{inc} and Ni_{wet} have very similar total acidity, 205,4 μmol/g_{sample} and 224,5 μmol/g_{sample}, respectively. This may indicate that the difference in products selectivity is not due to differences in total acidity of the Ni catalysts and it could be assigned to differences in the number of exposed Ni atoms and in the particle size. As was determined by TEM, the Ni_{inc} has bigger particles (4 nm-10 nm) with a mean Ni particle size of 6 nm while the Ni_{wet} has a Ni particle ranging between 4 nm–6 nm in diameter which could have affected the dispersion of the catalysts and its hydrogenolytic capacity.

Fig. 6 shows that the Ni_{inc} sample suffered the highest deactivation in comparison with the Ni_{wet} sample that was very stable during the 6 h of reaction. Raman spectra (Fig. 9) in the range of 1100 to 1800 cm^{-1} displayed the bands D and G (41) ascribed to carbon species. According to previous works (42-44), the D-band is associated to non-deactivating carbon (amorphous carbon) and the G-band is related to deactivating carbon (graphitic carbon).

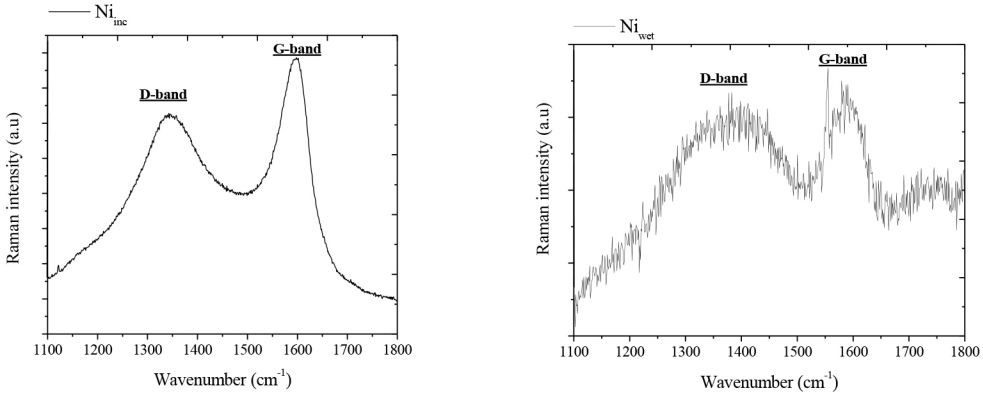

Figure 9. Raman spectra of the used Ni catalysts.

The carbon deposition on used Ni samples was determined by TPO, the Ni_{inc} sample showed 5,75 wt.% of carbon deposited and the Ni_{wet} sample showed 1,82 wt.%. In this case the dehydration route markedly contributed to the carbon deposition on the Ni_{inc} catalyst, as noted by previous works leading to the observed deactivation (45, 46). Although the acid sites contribute to the formation of carbon by the dehydration route, some contribution of metallic Ni to the formation of carbon by hydrogenolysis is also expected (2) and the carbon deposition on the catalyst also depends on the Ni particles size. It is well known that carbon deposition is also a consequence of the ability of the Ni to break the C-C bond producing CH_4 by hydrogenolysis reaction as could be the case of Ni_{wet} sample. However, as is observed in Fig. 6, the deactivation was deeper for the Ni_{inc} sample and it may be due to the higher amount of carbon deposited from the dehydration route.

3. CONCLUSIONS

The catalytic conversion of glycerol was investigated on Ni/γ-Al_2O_3 catalysts in gas phase. Two preparation methods, incipient wetness impregnation and wet impregnation, were applied to study their effects on the structure and performance of the catalysts. The selectivity and activity of the catalysts were affected by the preparation method employed. The hydrogenolysis and dehydration routes were evident for Ni_{inc} sample, the main products obtained were hydroxyacetone, pyruvaldehyde, pyruvic acid, methyl lactate, lactide, acetaldehyde and methane, while in the case of Ni_{wet} sample the selectivity to CH_4 was practically 100 % during the 6 h of reaction showing that the array of Ni surface atoms and its hydrogenolytic activity were predominant in this sample. Ni_{inc} sample presented a bigger particle size than Ni_{wet} sample which may have provoked the lower dispersion showed and the differences in selectivity. The Ni_{inc} sample suffered a bigger carbon deposition than the Ni_{wet} sample which is attributed to the dehydration route contribution.

4. ACKNOWLEDGMENTS

The author gratefully acknowledges the Universitat Rovira I Virgili (URV) and Universidad de Costa Rica for the financial support.

5. REFERENCES

1. Barrientos, J., Lualdi, M., Boutonnet, M., Järås, S. Deactivation of supported nickel catalysts during CO methanation. Appl Catal A. 2014;486:143-9.
2. Miranda, B. C., Chimentão, R. J., Santos, J.B.O., Gispert-Guirado, F., Llorca, J., Medina, F. *et al*. Conversion of glycerol over 10%Ni/γ-Al_2O_3 catalyst. Appl Catal B. 2014;147:464-80.
3. Huang, Y. -J., Barrett, B.T., Schwarz, J. A. The effect of solution variables on metal weight loading during catalyst preparation. Appl Catal. 1986;24:241-8.
4. Huang, Y.-J., Schwarz, J. A. The effect of catalyst preparation on catalytic activity: I. The catalytic activity of Ni/Al_2O_3 catalysts prepared by wet impregnation. Appl Catal. 1987;30:239-53.
5. Huang, Y.-J., Schwarz, J. A. The effect of catalyst preparation on catalytic activity: II. The design of Ni/Al_2O_3 catalysts prepared by wet impregnation. Appl Catal. 1987;30:255-63.
6. Bartholomew, C.H., Farrauto, R. J. Chemistry of nickel-alumina catalysts. J Catal. 1976;45(1):41-53.
7. Wang, S., G.Q.M., Lu. CO_2 reforming of methane on Ni catalysts: Effects of the support phase and preparation technique. Appl Catal B Environ. 1998;16:269-77.
8. Bezemer, G. L., Bitter, J. H., Kuipers, H. P. C. E., Oosterbeek, H., Holewijn, J. E., Xu, X. *et al*. Cobalt particle size effects in the Fischer-Tropsch Reaction studied with carbon nanofiber supported catalysts. J Am Chem Soc. 2006;128(12):3956-64.
9. Frelink, T., Visscher, W., van Veen, J.A.R. Particle size effect of carbon-supported platinum catalysts for the electrooxidation of methanol. J Electroanal Chem. 1995;382:65-72.
10. Morikawa, K., Shirasaki, T., Okada. M. Correlation among methods of preparation of solid catalysts, their structures, and catalytic activities. Adv Catal. 1969;20:97-133.
11. Campelo, J. M., García, A., Gutierrez, J. M., Luna, D., Marinas, J.M. $AlPO_4$-supported nickel catalysts. V. Effect of carrier, nickel precursor and nickel loading on particle size and I-hexene hydrogenation activity. Appl Catal. 1983;7:307-15.

12. Pinna, F. Supported metal catalysts preparation. Catal Today. 1998;41:129-37.
13. Kester, K.B., Falconer, J.L. J Catal. 1984;89:380.
14. Kester, B., Zagli, E., Falconer. J.L. Appl Catal. 1986;22:311.
15. Tsai, W., Schwarz, J.A., Driscoll, C.T. J Catal. 1982;78:88.
16. Huang, Y.-J., Schwarz, J.A. The effect of catalyst preparation on catalytic activity: III. The catalytic activity of Ni/Al_2O_3 catalysts prepared by incipient wetness. Appl Catal. 1987;32:45-57.
17. Boudart, M., McDonald, M.A. J Phy Chem. 1984;88(11):2185.
18. Huang, Y.-J., Schwarz, J.A. Effect of Catalyst Preparation on Catalytic Activity VII. The Chemical Structures on Nickel/Alumina Catalysts: Their Impact on the Formation of Metal-Support Interactions. Appl Catal. 1988;37:229-45.
19. Huang, Y.-J., Schwarz, J.A. Effect of Catalyst Preparation on Catalytic Activity V. Chemical Structures on Nickel/Alumina Catalysts. Appl Catal. 1988;36:163-75.
20. Huang, Y.-J., Schwarz, J.A. Effect of Catalyst Preparation on Catalytic Activity VI. Chemical Structures on Nickel/Alumina Catalysts: their Impact on the Rate-Determining Step in the Hydrogenation of Carbon Monoxide. Appl Catal. 1988;36:177-88.
21. Huang, Y.-J., Schwarz, J.A. The effect of catalyst preparation on catalytic activity: IV. The design of Ni/Al_2O_3 catalysts prepared by incipient wetness. Appl Catal. 1987;32:59-70.
22. Bartholomew, C.H., Pannell, R.B., Butler. J.L. Support and crystallite size effects in CO hydrogenation on nickel. J Catal. 1980; 65:335-347.
23. Gurbania, A., Ayastuya, J.L., Gonzalez-Marcosa, M.P., Herrero, J.E., Guilb, J.M., Gutierrez-Ortiz, M.A. Comparative study of $CuO–CeO_2$ catalysts prepared by wet impregnation and deposition–precipitation. Int J Hydrogen Energy. 2009;34:547-53.
24. Anderson, J. R., Pratt, K.C. Introduction to Characterization and Testing of Catalysts. New York: Academic Press; 1985.
25. Chen, I., Shiue, D.W. Reduction of Nickel-Alumina Catalysts. Ind Eng Chem Res. 1988;27(3):429-34.
26. Chen, I., Lin, S., Shiue, D. Calcination of Nickel/Alumina Catalysts. Ind Eng Chem Res. 1988;27(6):926-9.
27. Sietsma, J. R.A., Friedrich, H., Broersma, A., Versluijs-Helder, M., Jos van Dillen, A., de Jongh, P. E. *et al*. How nitric oxide affects the decomposition of supported nickel nitrate to arrive at highly dispersed catalysts. J Catal. 2008;260:227–35.
28. Li, G., Hu, L., Hill, J.M. Comparison of reducibility and stability of alumina-supported Ni catalysts prepared by impregnation and co-precipitation. Appl Catal A. 2006;301:16-24.
29. Richardson, J.T., Lei, M., Turk, B., Forster, K., Twigg, M.V. Reduction of model steam reforming catalysts: $NiO/\alpha\text{-}Al_2O_3$. Appl Catal A. 1994;110(2):217-37.
30. Velu, S., Gangwal, S.K. Synthesis of alumina supported nickel nanoparticle catalysts and evaluation of nickel metal dispersions by temperature programmed desorption. Solid State Ionics. 2006;177:803 – 11.
31. Velu, S., K. Suzuki, M. Vijayaraj, S. Barman, C.S. Gopinath. Appl Catal, B Environ. 2005;55:287–99.
32. Miranda, B.C., Chimentão, R.J., Szanyi, J., Braga, A.H., Santos, J.B.O., Gispert-Guirado, F. *et al*. Influence of copper on nickel-based catalysts in the conversion of glycerol. Appl Catal. 2015;166-167:166-80.
33. Lif, J., Odenbrand, I., Skoglundh, M. Sintering of alumina-supported nickel particles under amination conditions: Support effects. Appl Catal A. 2007;317:62-9.
34. Sing, K., Everet, D., Haul, R., Moscou, L., Pierotti, R., Rouquerol, J. *et al*. Reporting physisorption data for gas/solid systems with special reference to the determination of surface area and porosity. Pure Appl Chem. 1985;57:603-19.
35. Hadjiivanov, K., Mihaylov, M., Klissurski, D., Stefanov, P., Abadjieva, N., Vassileva, E. *et*

al. Characterization of Ni/SiO_2 catalysts prepared by successive deposition and reduction of Ni^{2+} ions. J Catal. 1999;185:314-23.
36. Zhu, X., Zhang, Y-p., Liu, C-j. CO adsorbed infrared spectroscopy study of Ni/Al_2O_3 catalyst for CO_2 reforming of methane. Catal Lett. 2007;118:306-12.
37. Mihaylov, M., Lagunov, O., Ivanova, E., Hadjiivanov, K. Determination of polycarbonyl species on nickel-containing catalysts by adsorption of CO isotopic mixtures. Top Catal. 2011;54:308-17.
38. Sinfelt, J.H. Specificity in catalytic hydrogenolysis by metals. Adv Catal. 1973;23:91-119.
39. Biloen, P., Helle, J. N., Verbeek, H., Dautzenberg, F. M., Sachtler, W.M.H. The role of rhenium and sulfur in platinum-based hydrocarbon-conversion catalysts. J Catal. 1980;63:112-8.
40. Soma-Noto, Y., Sachtler, W.M.H. Infrared spectra of carbon monoxide adsorbed on supported palladium and palladium-silver alloys. J Catal. 1974;32:315-24.
41. Hornésa, A., Bera, P., Fernández-García, M., Guerrero-Ruiz, A., Martínez-Arias, A. Catalytic and redox properties of bimetallic Cu–Ni systems combined with CeO_2 or Gd-doped CeO_2 for methane oxidation and decomposition. Appl Catal B. 2012;111-112:96-105.
42. de Sousa, F. F., de Sousa, H. S. A., Oliveira, A. C., Junior, M. C., Ayala, A. P., Barros, E.B. *et al*. Nanostructured Ni-containing spinel oxides for the dry reforming of methane: Effect of the presence of cobalt and nickel on the deactivation behaviour of catalysts. Int J Hydrogen Energy. 2012;37:3201-12.
43. Ferrari, A. C., Robertson, J. Interpretation of Raman spectra of disordered and amorphous carbon. Phys Rev B. 2000;61(20):14095-107.
44. Ferrari, A.C., Kleinsorge, B., Adamopoulos, G., Robertson, J., Milne, W.I., Stolojan, V. *et al*. Determination of bonding in amorphous carbons by electron energy loss spectroscopy, Raman scattering and X-ray reflectivity. J Non-Cryst Solids. 2000;266-269: 765-8.
45. Corma, A., Miguel, P. J., Orchilles, A.V. The Role of reaction temperature and cracking catalyst characteristics in determining the relative rates of protolytic cracking, chain propagation, and hydrogen transfer. J Catal. 1994;145:171-80.
46. Suprun, W., Lutecki, M., Haber, T., Papp, H. Acidic catalysts for the dehydration of glycerol: Activity and deactivation. J Mol Catal A: Chem. 2009;309:71-78.